A Numerical Sediment-Radionuclide Interaction Model for the Continental Shelf

A Report Prepared for the Applied Physics Laboratory, University of Washington

by

Miles G. McPhee

McPhee Research Company
450 Clover Springs Road
Naches WA 98937

email: miles@wolfenet.com
miles@apl.washington.edu

ABSTRACT

A boundary layer model based on the mixing length algorithm of McPhee [1994] is adapted to prediction of radionuclide concentrations for the relatively shallow environment of the continental shelf. Conservation equations for sediment species concentration and both sediment bound and dissolved radionuclide concentration are combined with similar conservation equations for momentum, temperature (heat) and salinity. Three idealized storm situation for intermediate depth water are considered and analyzed. In the first two, initially "clean" water overlies radioactive sediment which is stirred into the water column by bottom turbulent stress as the storm develops. In the first, initial stratification is strong enough that a two-layer density structure persists throughout the storm, confining the sediment and radionuclides mainly to the bottom layer. In the second, the initial stratification is weak enough to allow complete mixing during the storm, so that both dissolved and sediment bound radionuclides may interact with the surface, and could, for example, be incorporated into sea ice. In the third scenario, radioactively contaminated water interacts with initially "clean" sediment, which is stirred up during the storm and "scavenges" dissolved radionuclides.

1. Introduction

The purpose of this study is to demonstrate a model for turbulent transfer of suspended sediment in a continental shelf environment at intermediate depths (~50 to 100 m), and to assess the movement of radionuclides associated with sediment transport as part of a broader study of the fate of radionuclides in the Arctic. The main thrust is to construct a framework for assessing quantitatively conditions under which an appreciable off- ar along-shelf flux of radioactively contaminated material might occur. The model provides for migration of radionuclides between sediment bound and dissolved states, and illustrates how radioactive material might move from sediment to initially uncontaminated water during sediment transport events, or conversely how initially clean sediment can scavenge radionuclides from contaminated water. The simulations presented here are highly idealized, intended to illustrate principles rather than reproduce observed events. The purpose is to understand the physical underpinnings of transport of radioactive material on the shelf, and to develop parameterizations of the process for use in more extensive three-dimensional models.

The report is organized as follows. In Section 2, equations and boundary conditions for the time-dependent, horizontally homogeneous model are developed, along with discussion of the relevant forcing. The model uses turbulence closure based on a mixing length algorithm [McPhee, 1994] developed from extensive flux measurements in the boundary layer under drifting sea ice. It realistically incorporates the effects of stabilizing or destabilizing due to freezing or melting at the surface, and due to scouring of sediment at the seafloor. In addition, it accounts for the large increase in mixing efficiency (eddy diffusivity) associated with intense boundary stress.

Smith and Hopkins [1972] discussed near bottom currents measured on the Washington continental shelf and combined them with theoretical treatment to arrive at rough estimates of offshore sediment transport. They reported current velocities in excess of 0.6 m s^{-1} on the Washington shelf, and stressed that nearly all of the sediment transport occurs during infrequent, severe storms. Prompted by these observations, an idealized severe storm event is simulated under differing conditions of initial stratification and initial radionuclide distribution in Section 3. Three model scenarios are considered. In the first, an initial stratification is specified that is strong enough to maintain a two-layer density structure throughout the storm, limiting most of the sediment and radionuclide concentrations to the lower layer. In the second study, upper layer salinity is increased so that stratification breaks down midway through the storm, bringing much higher sediment concentrations into surface contact with the ice, with its potentially high mobility. In both cases, radioactivity is initially confined to the bottom sediment. A variation is provided by the third simulation, where “clean” sediment is stirred into an initially radioactive water column, in order

to assess scavenging as the radionuclides bind to the suspended sediment and settle to the bottom. Results are discussed and summarized in Section 4.

2. The Model

2.1 Equations

The model comprises numerical solution of the following set of coupled, partial differential equations:

$$\begin{aligned}
\hat{u}_t + if\hat{u} &= (-K\hat{u}_z)_z \\
S_t &= (-\alpha K S_z)_z \\
T_t &= (-\alpha K T_z)_z \\
C_t^{(1\ldots n)} - \bar{w} C_z^{(1\ldots n)} &= (-\alpha K C_z^{(1\ldots n)})_z \\
N_t^{b(1\ldots m)} - \bar{w} N_z^{b(1\ldots m)} &= (-\alpha K N_z^{b(1\ldots m)})_z + Q^{b(1..m)} \\
N_t^{w(1\ldots m)} &= (-\alpha K N_z^{w(1\ldots m)})_z + Q^{w(1..m)}
\end{aligned} \tag{1}$$

where subscripts denote partial differentiation, $\hat{u}$ is complex horizontal velocity, f is the Coriolis parameter, K is eddy viscosity, S is salinity, α is the ratio of scalar eddy diffusivity to eddy viscosity, T is temperature, C is sediment volume concentration and the series (1...n) represents different sediment species (only one species is considered here), $\bar{w}$ is sediment settling velocity (positive downward), N^b is sediment-bound radionuclide concentration, with units Bq m^{-3}, for radioisotope species 1 through m, and N^w is dissolved sediment concentration (also with units Bq m^{-3}). Q^b and Q^w are source terms (i.e., within the water column) for bound and dissolved sediments, respectively, encompassing both mobility and radioactive decay. Eddy viscosity is given by $K = u_* \lambda$ where u_* is the square root of the local Reynolds stress magnitude and λ is the mixing length, computed for top and bottom mixed layers according to the algorithm presented in Fig. 15 of McPhee [1994], and in the stratified pycnocline using similarity concepts described by McPhee [1981; 1994]. When the boundary layer is statically unstable, in rare situations where the convective turbulent scaling velocity $w_* = (\lambda \langle w'b' \rangle_b)^{1/3}$ ($\langle w'b' \rangle_b$ is buoyancy flux at the

boundary) is greater than u_*, it replaces friction velocity in the eddy viscosity determination [McPhee, 1996].

The equations are solved implicitly on a vertical grid with 100 levels, using a leap-frog method in time.

2.2 The concentration flux boundary condition

By analogy with the formulation of boundary conditions at the ice-ocean interface [e.g., McPhee, 1990], consider a finite control volume following the bottom surface which moves with an erosion rate, $\dot{d}$, chosen to be positive downward. Assuming no mass storage in the control volume we have:

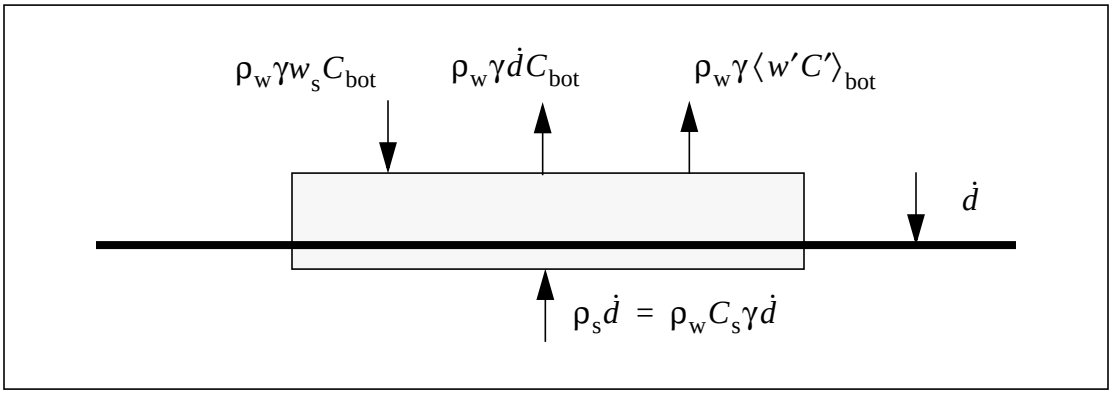

Figure 1. Schematic of the boundary condition for a particular sediment species, where ρ_w is water density, w_s is the sediment "settling" velocity (positive downward), γ is the specific gravity of solids comprising the sediment, C_{bot} is the concentration at the lower boundary of the model (upper boundary of the control volume), and C_s is the volume concentration of the sediment entering the control volume from below.

An equation for $\langle w'C' \rangle_{bot}$, the turbulent concentration flux at the lower boundary of the model, is provided by the mass balance:

$$\langle w'C' \rangle_{bot} = (C_s - C_{bot})\dot{d} + w_s C_{bot} \qquad (2)$$

C_{bot} is obtained from the logarithmic C profile near the bottom boundary. For convenience we will identify the lower boundary of the sediment transport model with that of the turbulence mod-

el, namely z_{0b}.

A rigorous treatment requires separate flux boundary condition equations for each sediment classification. Lacking detailed knowledge of the bottom characteristics, however, we assume that the suspended sediment load can be characterized by single values for C_s, γ, and w_s. Unfortunately, there are few data on which to base estimates of the rate of erosion on the continental shelf for storm conditions. There is justification from laboratory studies [Mehta, 1988] for assuming that erosion rate is proportional to the difference between the bottom stress and a threshold stress below which little erosion occurs:

$$\frac{\dot{d}}{\dot{d}_M} = \frac{(\tau_b - \tau_c)}{\tau_c} \tag{3}$$

where τ_b is the bottom stress, τ_c is the threshold stress and $\dot{d}_M$ is a proportionality constant. Mehta [1988, Table 4] lists several estimates of erosion rate constants and shear strength; the most appropriate for this study appears to be estuarial mud, for which $\tau_c = 0.2$ Pa and $\dot{d}_M = 1\times10^{-8}$ m s^{-1}.

The impact of sediment loads, carrying a buoyancy anomaly, on turbulent structure of the boundary layer has been discussed by, among others Smith [1977] and Trowbridge and Kineke [1994]. Combining (3) with a bed stress based on maximum currents provides an order-of-magnitude estimate of the impact of the concentration flux on the stability of the bottom boundary layer. Bottom stress, $\hat{\tau}_b = u_{*b}\hat{u}_{*b}$, is obtained from a Rossby similarity formula [McPhee, 1979; 1990].

$$\frac{\hat{U}_g}{\hat{u}_{*b}} = \hat{\Gamma} = \frac{1}{\kappa}(\log Ro_* - 1.91 - 2.12i) \tag{4}$$

where overhats indicate vector (complex) quantities and $Ro_* = u_{*b}/(fz_{0b})$ is the bottom friction Rossby number. Using $z_{0b} = 0.01$ m for bottom roughness, (3) yields $u_{*b} = 0.032$ m s^{-1} for $U_g = 0.7$ m s^{-1}. For the erosion parameters associated with estuarial mud, (2) provides an erosion rate of 4.3×10^{-8} m s^{-1}. If the bottom concentration flux is approximately equivalent to the erosion rate (i.e., $C_{bot} \ll C_s \approx 1$), we have $\langle w'b' \rangle_b \approx g(\gamma - 1)\dot{d} \approx 0.5\times10^{-6}$ m^{2}s^{-3}. For the ocean this is a

large number, corresponding, for example, to the stabilizing surface buoyancy flux associated with an ice melt rate of around 25 cm d^{-1}. Its effect on turbulence is ameliorated, however, by the fact that the large buoyancy flux occurs only in combination with large bottom stress. The associated Obukhov length (when turbulence scales are smaller than the Obukhov length, buoyancy is important in the turbulent kinetic energy equation) is:

$$L = \frac{u_{*b}^3}{\kappa \langle w'b' \rangle_b} \approx 160 \text{ m} \tag{5}$$

which is larger than the total depth over the continental shelf. By contrast, if ice were melting at 25 cm d^{-1} with a typical ice-ocean stress of 0.1 Pa, the corresponding Obukhov length would be around 5 m and the boundary layer turbulence would be significantly altered by buoyancy. Thus, it appears that buoyancy flux associated with sediment scouring will seldom have overriding impact on turbulence near the seafloor during storms. Nevertheless, it may indeed affect vertical mixing higher in the water column, and the model is designed to include buoyancy effects associated with the sediment concentration gradient.

2.3 Radionuclide Concentration Equations

A sediment transport model is sufficient to determine offshore transport and near surface concentrations of radioactive materials only if radionuclides are tightly bound to sediments. In practice the mobility of a radionuclide between sediment-bound and dissolved-in-sea-water states is relatively large, and is important in two scenarios. First, if nonradioactive seawater exists over a previously deposited bed of radioactive sediment, it seems physically plausible that transfer of radionuclides will occur mainly in major sediment transport events. Once the radionuclides are freed from the sediments, they are much more mobile. Second, if radioactive seawater interacts with relatively “clean” suspended sediment, for many radionuclides the sediment will be an efficient scavenger and major sediment events will decrease radioactivity in the water column.

Our approach is to simplify as much as possible the modeled exchange of radionuclides between the suspended sediment and water. We carry scalar equations for concentrations of both sediment bound radionuclides, N^b, and dissolved radionuclides, N^w, with units Bq m^{-3} (1 curie = 3.7×10^{10} Bq or disintegrations per second). In the absence of vertical fluxes, the radionuclide concentration equations in (1) reduce to:

$$N^{b}_{t} = Q^{b}$$
$$N^{w}_{t} = Q^{w} \tag{6}$$

Here we assume that the radionuclide half-life is long enough to neglect radioactive decay, in which case $Q^{b} = -Q^{w}$.

For water in contact with radioactive sediment, the factor $\bar{K}_{d}$ expresses the equilibrium ratio of concentrations of bound radionuclides to those in solution, i.e., $R^{b}/R^{w} \rightarrow \bar{K}_{d}$ for long times, where $\bar{K}_{d}$ has units ml g^{-1} (equal to l kg^{-1}). Let R^{b} equal the concentration of bound radionuclides, expressed as Bq kg^{-1}, and R^{w} equal the concentration of dissolved radionuclides as Bq l^{-1}. The total radionuclide concentration expressed as Bq m^{-3} is

$$N^{tot} = N^{w} + N^{b} = 10^{3} \times R_{w} + \rho_{w}\gamma C R_{b} \tag{7}$$

since $N^{w} = R_{w} \times (10^{3}\text{liter/m}^{3})$. $\bar{K}_{d}$ varies strongly with water salinity and radioisotope. During a sediment suspension event, it is unlikely that the bound and dissolved radionuclides will be in equilibrium throughout the water column, thus the coupled source terms in (6) must account for the tendency to adjust the concentrations toward the equilibrium ratio, $\bar{K}_{d}$. We assume that to first order, the process involved varies directly with the departure from equilibrium, and inversely with a time constant, possibly dependent on the particular radionuclide:

$$Q^{w} = -\frac{\Delta N^{w}}{\Im} \tag{8}$$

where $\Im$ is the time constant ("e-folding time") and

$$\Delta N^{w} = N^{w} - N^{w}_{\infty} = N^{w} - \frac{N^{tot}}{1 + (\rho_{w}\gamma C/10^{3})\bar{K}_{d}} \tag{9}$$

A rough estimate of the time constant $\Im$ may be made from the adsorption time series for ^{134}Cs from Fig. 3 of Oughton et al. [1995]. The homogeneous conservation equations (6) reduce to sim-

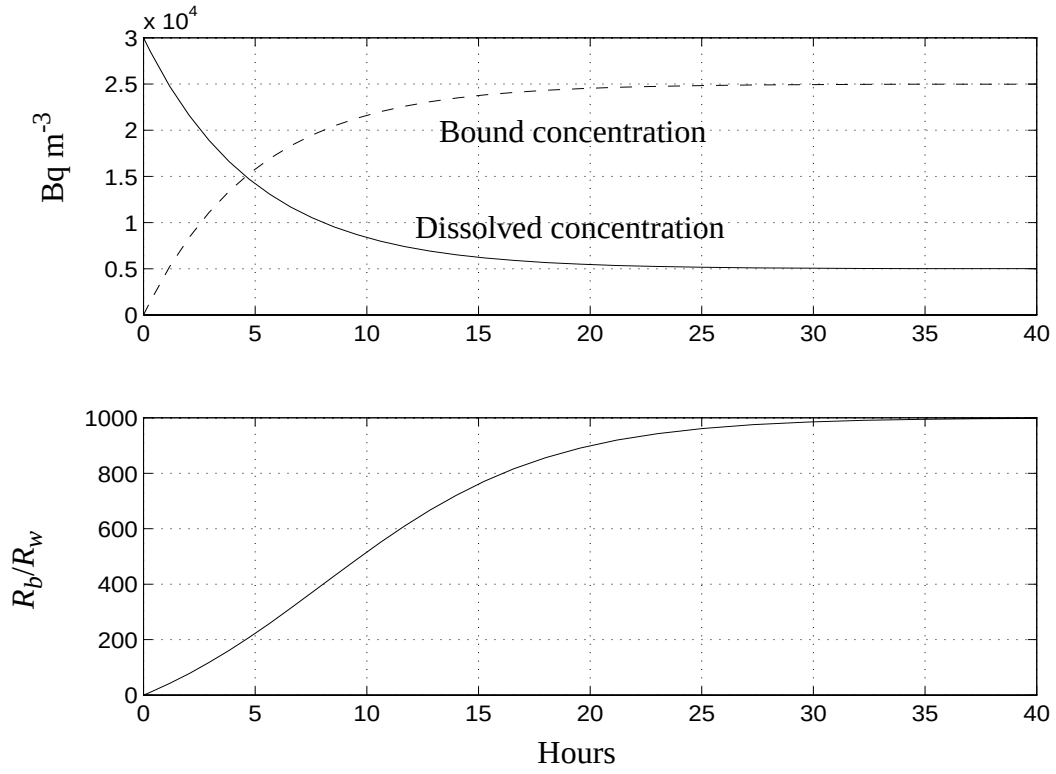

Figure 2. Hypothetical stirred radioisotope adsorption experiment assuming a rate equation given by (10), with a time constant of 5 h.

ple first-order differential equations, e.g.,

$$N^{\mathrm{w}}{}_t = -\frac{\Delta N^{\mathrm{w}}}{\Im} \tag{10}$$

Oughton et al. [1995] found that with undisturbed samples of the tracer ^{134}Cs, the ratio $R^{\mathrm{b}}/R^{\mathrm{w}}$ reached half $\overline{K}_{\mathrm{d}}$ (equilibrium value) after about 100 h, but that gentle shaking decreased this time by a factor of ten. Here we assume the ratio reaches half $\overline{K}_{\mathrm{d}}$ after about 10 hrs. The tests were done with 10 g (dry weight sediment) in 2 l of water, to which we assign an initial total dissolved radioactive concentration of 3×10^4 Bq m^{-3} (i.e., 30 Bq per liter). For a continuously stirred mixture, the volume sediment concentration is $C = 2.5\times10^{-3}$, assuming $\gamma = 2$. The added sediment is assumed to be nonradioactive. The solution of (10) for these conditions is graphed in Fig. 2, for $\Im = 5$ h. The isotope concentration ratio reaches half its equilibrium value ($\overline{K}_d = 1000$ ml g^{-1})

after about 10 h. This crude approximation illustrates that adsorption and mobilization probably occur fairly rapidly.

2.4 Radionuclide Flux Boundary Condition

The flux of radionuclide concentration entering or leaving the ocean model is assumed to be entirely bound to the sediment. No provision is made for diffusion of dissolved concentration

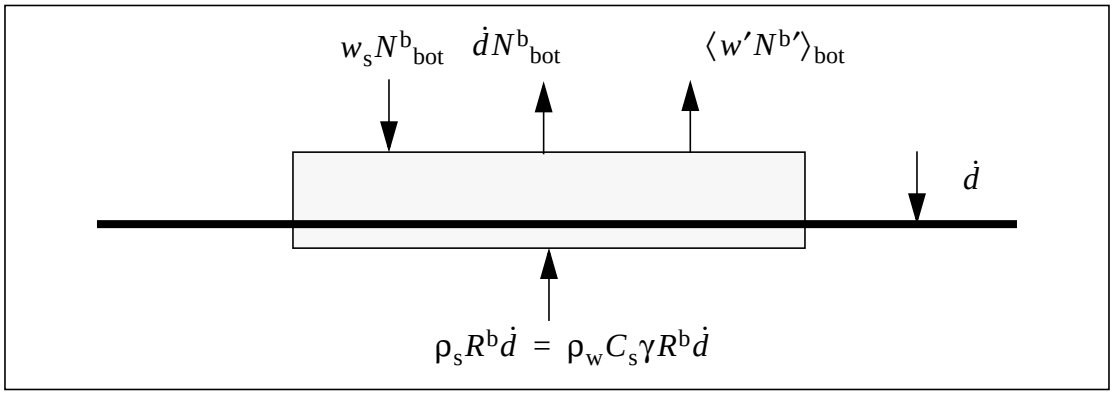

Figure 3. Boundary condition schematic for a sediment-bound radionuclide species with radioactivity R^b (Bq kg^{-1}) attached to sediment with solid volume concentration C_s.

across the interfaces, nor for radioactive decay, although the latter is easily incorporated into the source terms. In the long run, the ocean model should incorporate a frazil ice model at the surface which would provide the means for uptake into the ice cover. A similar approach to that used for the concentration equation is used (Fig. 2) so that the boundary condition for bound radionuclides corresponding to (2) is

$$\langle w' N^{b\prime} \rangle_{bot} = (\rho_w C_s R^b \gamma - N^b{}_{bot}) \dot{d} + w_s N^b{}_{bot} \tag{11}$$

where R^b is expressed in consistent units (Bq kg^{-1}, *not* Bq g^{-1}), and $N^b{}_{bot}$ is the bound concentration at the top of the sediment control volume (i.e., z_{0b} above the bottom), obtained from the near bottom grid point via the law of the wall. At the upper boundary, we assume that the sediment radionuclide concentration flux is zero

3. Model Simulations

3.1 Stratified Storm Surge Scenario

Since previous studies [e.g., Smith and Hopkins, 1972] have shown that the most significant sediment transport on continental shelves occurs mainly during severe storms, the emphasis here is on extreme events. To adapt a one-dimensional model forced by wind stress at the surface to the problem of bottom sediments in a (possibly stratified) shelf environment, we consider the approach developed by Ekman in his classic paper [1905]. He introduced the concept of a *slope current system*, which can be applied directly to the problem at hand. Along a continental shelf that is relatively uniform in the alongshore direction, storm-driven onshore (or offshore) Ekman mass transport in the surface boundary layer will be balanced eventually by offshore (or onshore) mass transport in the bottom boundary layer. For a steady system, the stress at the bottom must be large enough to produce the required offshore transport. The system reaches this state by raising or lowering sea level at the coast, tilting the sea surface across the shelf enough to create a geostrophic current in the fluid interior just sufficient to produce the required bottom stress. In an amazing intuitional leap, Ekman used alongshore current measurements and setup of sea level on the Norwegian coast during storms to make the first credible estimates of eddy viscosity in the ocean.

For a particular location on the continental shelf, the most severe offshore sediment transport will occur when the wind is directed alongshore with the coast *cum sole*, and sea surface tilt is fully developed to produce balanced mass transports in the upper and lower boundary layers. Examples below will illustrate scenarios approximating this situation, which are amenable to one-dimensional modeling.

Here we examine a plausible case for extensive sediment transport in the bottom boundary layer by simulating a powerful storm of 5 days duration, which after a short lag time sets up an onshore pressure gradient resulting in a strong alongshore geostrophic current.

Geostrophic velocity is $\hat{U}_g = -ig\nabla\eta / f$, where g is the acceleration of gravity and $\nabla\eta$ is the horizontal sea surface gradient. It is estimated from the storm surge as follows. The system will tend toward a steady state with offshore transport in the bottom boundary layer balancing onshore transport in the surface boundary layer. Relative to the geostrophic flow in the interior, the surface transport is

$$\hat{M}_s = \int_{-h_{sl}}^{0} (\hat{u} - \hat{U}_g)\,dz = -i \cdot \hat{\tau}_s / f \qquad (12)$$

where $\hat{\tau}_s$ is the stress at the surface and h_{sl} is the depth of the upper boundary layer. Choosing the

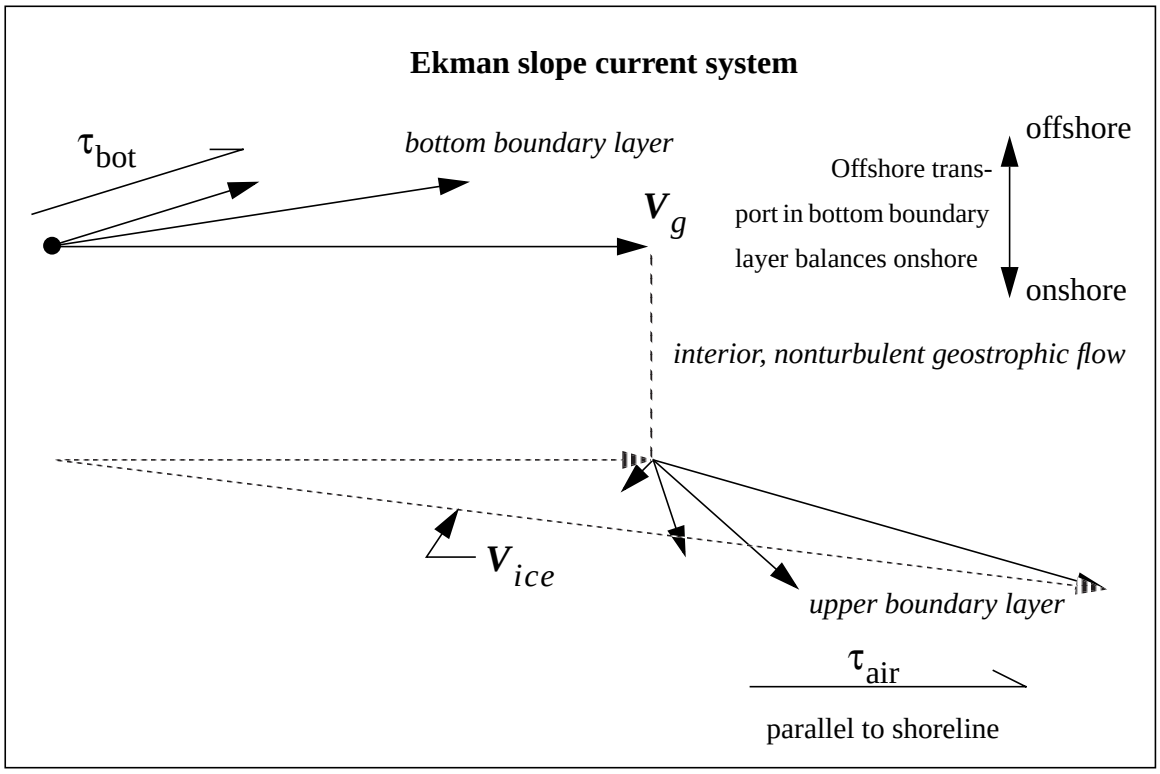

Figure 4. Schematic of the slope current system for an ice covered coastal ocean in the northern hemisphere, illustrating how wind forcing induces large currents through the entire water column, even if the ocean is stratified.

real and imaginary axes to lie alongshore and offshore respectively, the maximum onshore transport occurs when the stress is real and positive: $\hat{\tau}_s = \tau_s$. With no alongshore pressure gradient, U_g is constrained to the real axis. Transport in the bottom boundary layer, relative to geostrophic flow, is

$$\hat{M}_b = i\hat{\tau}_b / f = \frac{U_g^2}{f|\hat{\Gamma}|^2} e^{i\left(\frac{\pi}{2}+\beta\right)} \tag{13}$$

where we have used the Rossby similarity law, (3), and β is the bottom boundary layer turning angle, $\beta = \tan^{-1}(Im(\hat{\Gamma})/Re(\hat{\Gamma}))$. From balancing transports along the imaginary (offshore) axis, geostrophic flow tends toward the limit

$$U_{gmax} = |\hat{\Gamma}| \sqrt{\frac{\tau_s}{\cos\beta}} \qquad (14)$$

Ekman [1905] also investigated the time required for sea surface slope to develop in response to wind. By simple mass conservation arguments, he formulated and solved a partial differential equation analogous to the heat conduction equation, showing that for reasonable values of eddy viscosity (he used 0.04 $m^2 s^{-1}$) it took about 8 hrs for the sea surface slope to reach 70% of the steady-state value required for balanced transport, at a distance 100 km from shore.

Given this background, the strategy here is to force the one-dimensional model with an idealized, cosine-bell storm with peak winds of 25 m s^{-1} and a geostrophic velocity (sea-surface tilt) forcing with the same shape in time, except lagged by half a day. Its maximum value equals 80% of the fully developed balance given by (14). The water column is 70 m deep, with upper and lower mixed layers initially of equal extent, separated by a narrow pycnocline. Although the model considers the heat and mass balance at the ice/ocean interface, including buoyancy effects on turbulence, here we assume that the water column is at freezing and that freezing or melting of the ice is negligible. One bottom sediment species is considered (C_s = 1) with γ = 1.8, $\dot{d}_M = 1\times10^{-8}$ m s^{-1}, and τ_c = 0.2 Pa [Mehta, 1988]. A settling velocity of 1.16×10^{-4} m s^{-1} (10 meters per day) is specified.

We simulate concentrations of two radionuclide tracer species for which estimates of $\bar{K}_d$ have been made by Oughton et al. [1995]: ^{134}Cs ($\bar{K}_d \approx 1000$ ml g^{-1}) and ^{85}Sr ($\bar{K}_d \approx 11$ ml g^{-1}).

In the first model run, the salinity difference between the upper and lower layers is 2 on the practical salinity scale (2 psu). Initially the water column is uncontaminated $N^{w(1,2)} = 0$. with radionuclide concentrations, $R^{b(1,2)} = 20$ Bq kg^{-1}. The storm starts from quiescent conditions at t = 0 days, with the wind rising to 25 m s^{-1} at t = 2.5 days and falling back to zero at t = 5 days. The geostrophic current lags by 0.5 days, and peaks at 0.75 m s^{-1}. Fig. 5 summarizes the computed boundary forcing for Run 1. Surface stress follows the wind stress closely, and bottom stress follows the lagged geostrophic current. The maximum sediment flux corresponds to an erosion rate of around 1 cm per day. Note that at a level 5 m above the seaflloor, the flux Richardson number (Ri_f is the ratio of buoyancy to shear production of turbulent kinetic energy) is always less than about 0.02, implying that the impact of sediment buoyancy flux on turbulence near the

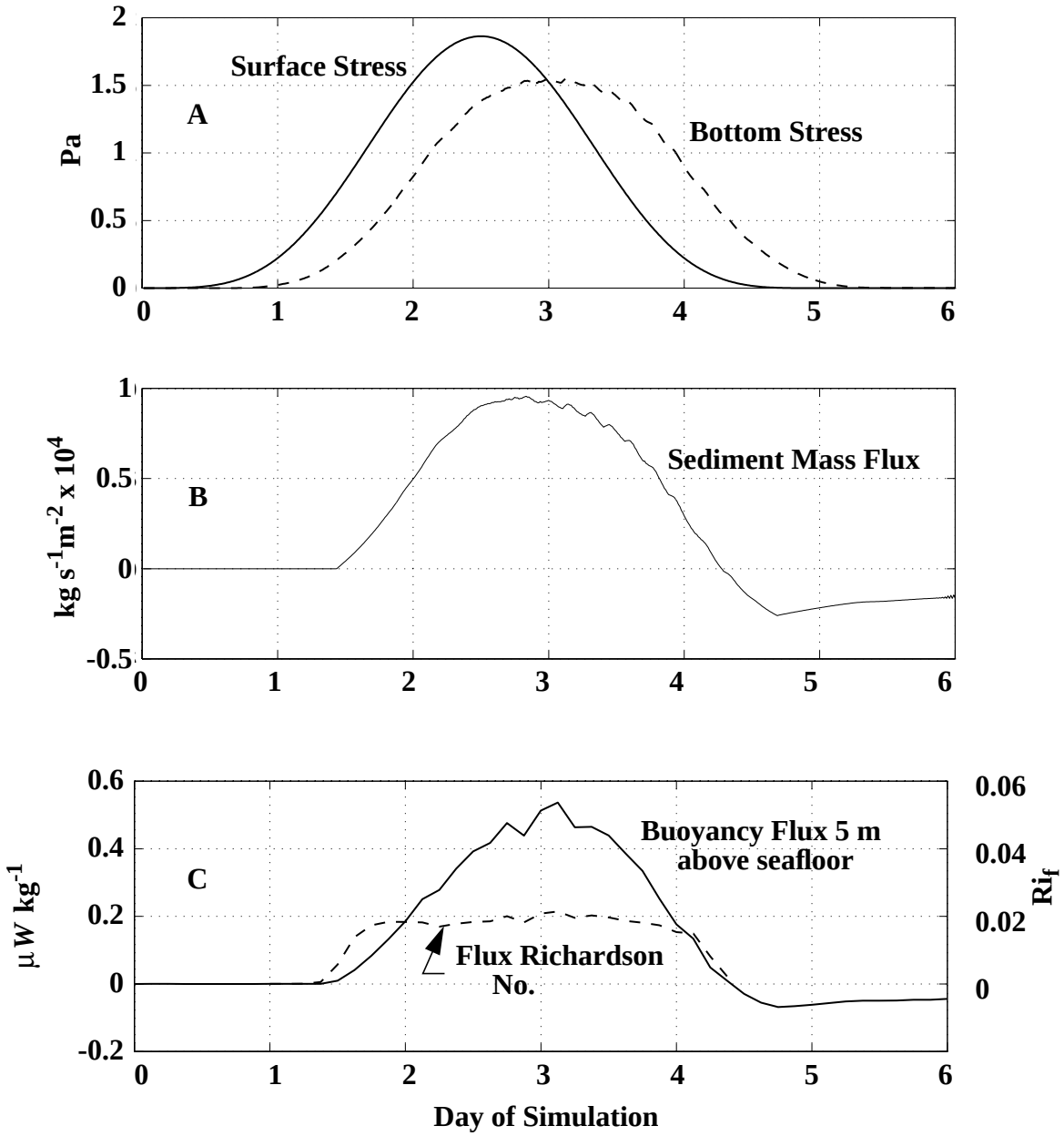

Figure 5. Run 1 with stratification maintained through the simulated storm. A. Boundary shear stresses. B. Seafloor sediment mass flux. C. Buoyancy flux and flux Richardson number (ratio of shear production to buoyancy production) 5 m above the seafloor in the bottom boundary layer.

bottom is small.

Evolution of the salinity (density) structure during the storm is shown by perspective view in Fig. 6A,. which is shaded by friction velocity to indicate the intensity of turbulent stress. At the

peak of the storm, he system remains stratified with vigorously turbulent upper and lower boundary layers separated by a narrow pycnocline in which u_* is substantially reduced, as indicated by redder colors. Note, however, that each boundary layer erodes the pycnocline, so that the density contrast between the layers is much less by the end of the storm. The sediment concentration field is shown in perspective view in Fig. 6, where the shading in this case represents the offshore velocity component. Offshore transport is largest where the concentration is high, colored blue. Red colors in the upper layer indicate the large onshore mass flux component required by the Ekman slope current system. The sediment is mostly confined to the bottom layer, but some "leaks" through by mixing in the pycnocline, and in fact there is limited shoreward transport in the upper boundary layer After the storm abates, the sediment begins settling back out

3.2 Thoroughly Mixed Storm Surge Scenario

A second run, identical to the first except that the initial change in salinity across the pycnocline is 1 psu, illustrates what happens when the overall stratification is too weak to withstand the storm's intense mixing. Here the water column mixes completely about midway through the storm. Bottom stress is enhanced when turbulence transmits the wind stress through the entire column (Fig. 7A). Under the increased stress the erosion rate also increases (Fig 7B), and again the flux Richardson number remains relatively small near the bottom, despite maximum stabilizing buoyancy flux approaching 1×10^{-6} W m^{-3}. The salinity perspective (Fig. 8A) shows the collapse of the two-layer system, and also reveals that the stress becomes more or less uniform through the water column after the stratification is eliminated. The sediment concentration also mixes thoroughly (Fig. 8B), and the offshore current structure becomes much more uniform after the salinity stratification disappears.

One implication of the breakdown in stratification is that the local offshore sediment transport changes dramatically. Since sediment is much more evenly distributed in the water column,

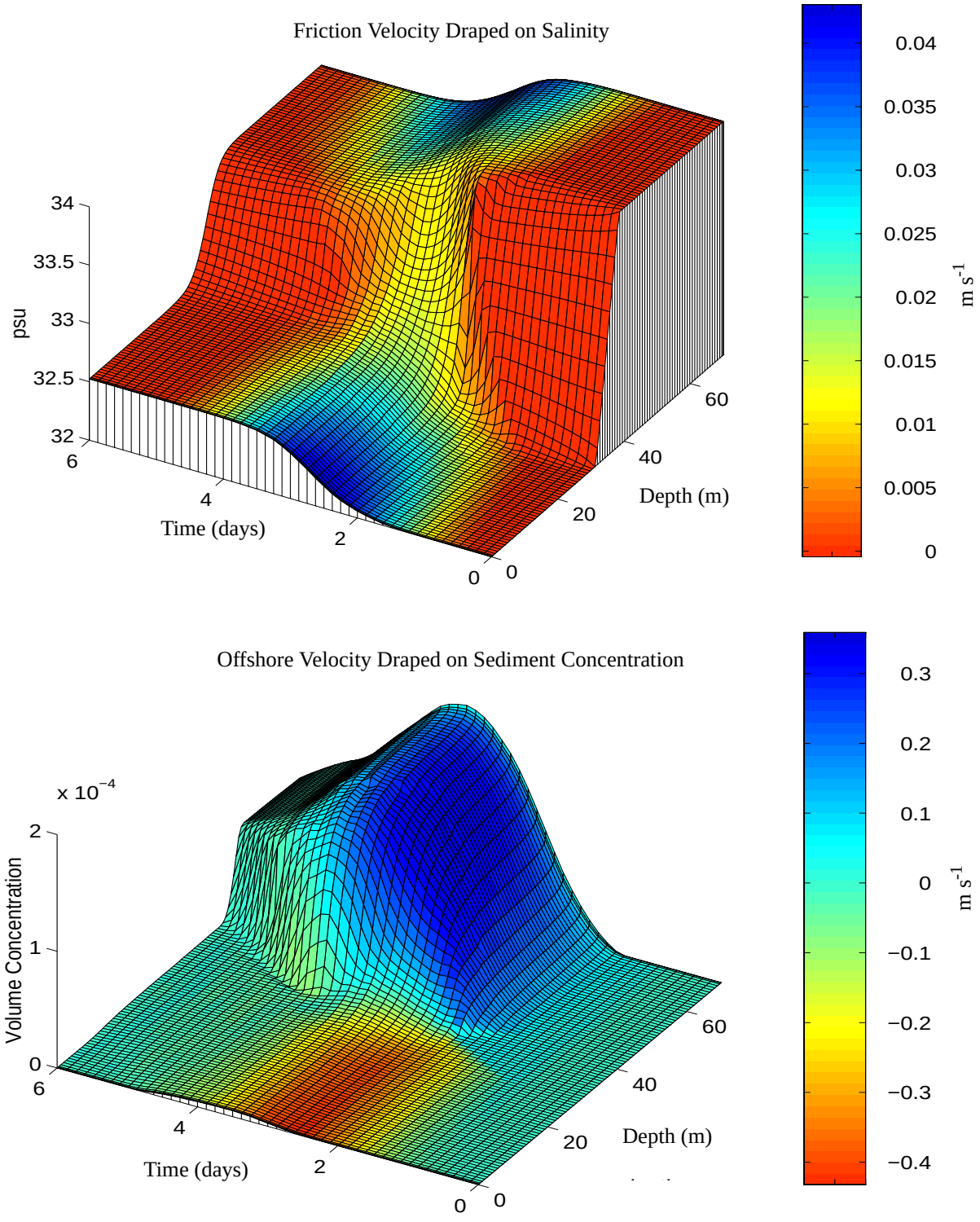

Figure 6. Depth-time perspective view from Run 1 of: (A) friction velocity draped on salinity; and (B) offshore velocity draped on volume sediment concentration.

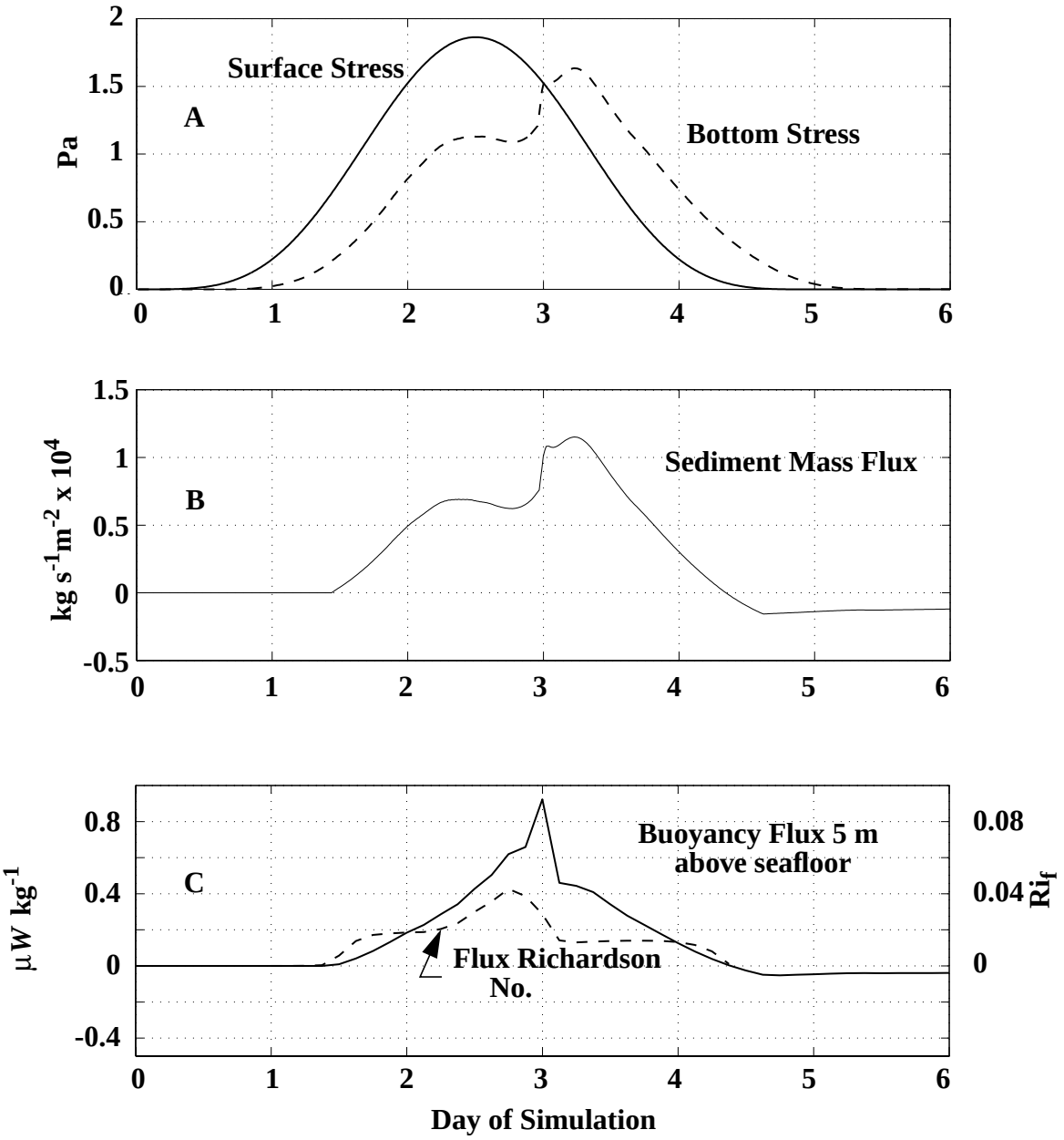

Figure 7. Run 2 with stratification breaking down midway through the storm. A. Boundary shear stresses. B. Seafloor sediment mass flux. C. Buoyancy flux and flux Richardson number (ratio of shear production to buoyancy production) 5 m above the seafloor in the bottom boundary layer.

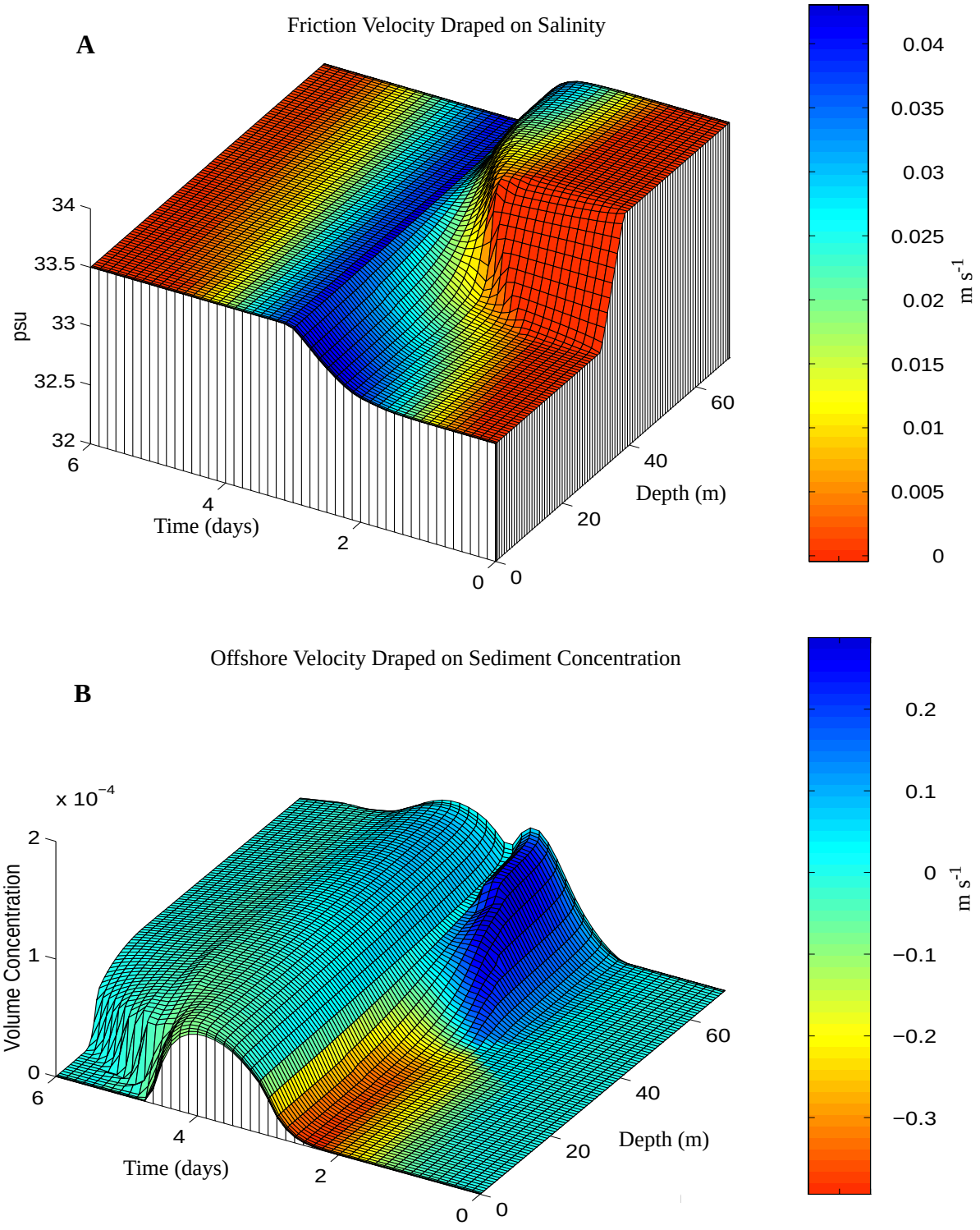

Figure 8. Depth-time perspective view from Run 1 of: (A) friction velocity draped on salinity; and (B) offshore velocity draped on volume sediment concentration.

wind driven onshore Ekman transport near the surface carries a large sediment load shoreward.

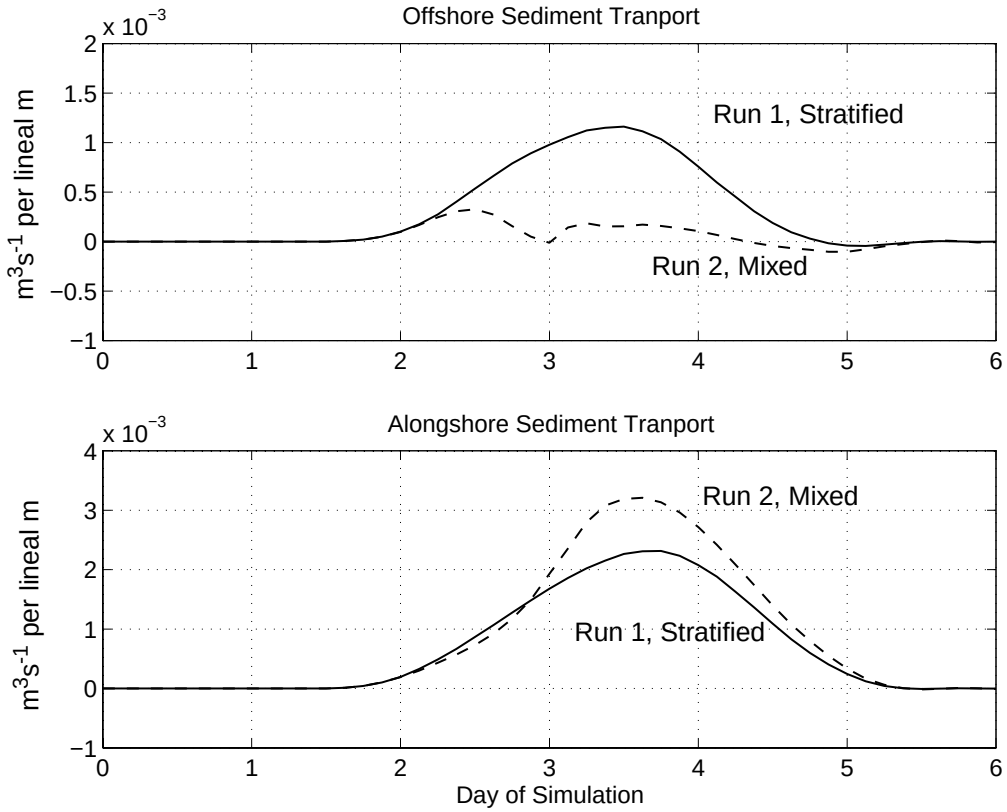

Figure 9. Offshore (A) and alongshore (B) vertically integrated sediment transport for the severe storm scenarios. Solid curve is for Run 1, with initial stratification sufficient to maintain two layers through the storm, and dashed curve is for Run 2, where the initially weaker stratification breaks down after about 3.25 days

The vertically integrated products of sediment concentration with *v* and *u* velocity components (offshore and alongshore in the wind direction, respectively) are shown in Fig. 9. The offshore transport is much reduced in the well mixed case, while alongshore transport is somewhat enhanced. Proper assessment of the actual transport on a specific continental shelf would require a much more sophisticated model, but qualitatively, the present results show that movement of sediments seaward is probably much more efficient when the water column remains stratified. On the other hand, the fully mixed case brings radioactive material into direct contact and possible uptake in the ice cover.

3.3 Radionuclide Concentrations

The radionuclide concentration in the water column depends on both the amount and dis-

tribution of sediment during and after the storm event, and on the mobility of the radioactive material between water and sediment, i.e., how strongly a radionuclide is bound to sediment. We consider two tracer radionuclides that differ mainly in their affinity for binding to sediment particles.

Example 1 (Fig. 10) shows bound and dissolved radionuclide concentrations for ^{134}Cs, with relatively strong sediment binding $\overline{K}_d$ = 1000 mg ml^{-1}, were calculated for the strong initial stratification case. As stress increases, sediment flux from the bottom begins mixing into the lower layer carrying radioactivity with it. Despite the relatively strong binding, dissolved concentration nevertheless dominates the total radionuclide concentration in the aftermath of the storm, so that as the sediment concentration decreases due to settling (Fig. 6B) it leaves much of the radioactive nuclide in the water column. Since turbulent diffusion between the layers is limited by persistent stratification (Fig. 6A), most of the contamination remains in the lower layer although a small amount “leaks” through the pycnocline.

Example 2 (Fig. 11) is the same as Example 1, except that a more soluble tracer species: ^{85}Sr, was considered. The concentration and duration of bound sediment radioactivity is smaller so that by the end of the simulation, nearly all of the radioactivity in the water column is in a dissolved state.

Example 3 (Fig. 12): This case is like example 1, except that the initial stratification is weaker and complete mixing of the water column occurs during the storm. The maximum concentration in the upper layer is enhanced considerably for both bound and dissolved radionuclide concentrations. Note that there is a time from about day 3 to day 4.5 of the simulation when bound concentrations in the upper few meters approach 3-4 Bq m^{-3}. Frazil ice crystals nucleating about sediment particles at this time would constitute a relatively efficient uptake mechanism for incorporating radioactive material into the ice cover.

Example 4 (Fig. 13): This is like the previous example, except with a more soluble tracer species. In this case the “window” for ice uptake is reduced because by the time sediment arrives at the surface, less of its radioactivity remains in the bound state.

Example 5 (Fig. 14): This case represents a scenario in which initially contaminated water carrying a radionuclide species in the dissolved state overlies an uncontaminated seafloor. A storm imposed on initially weak stratification similar to examples 3 and 4 is simulated, except that after the storm (day 5.5) weak surface and bottom stress are maintained. A radionuclide with relatively strong sediment binding is specified. The “scavenging” capability is clear.

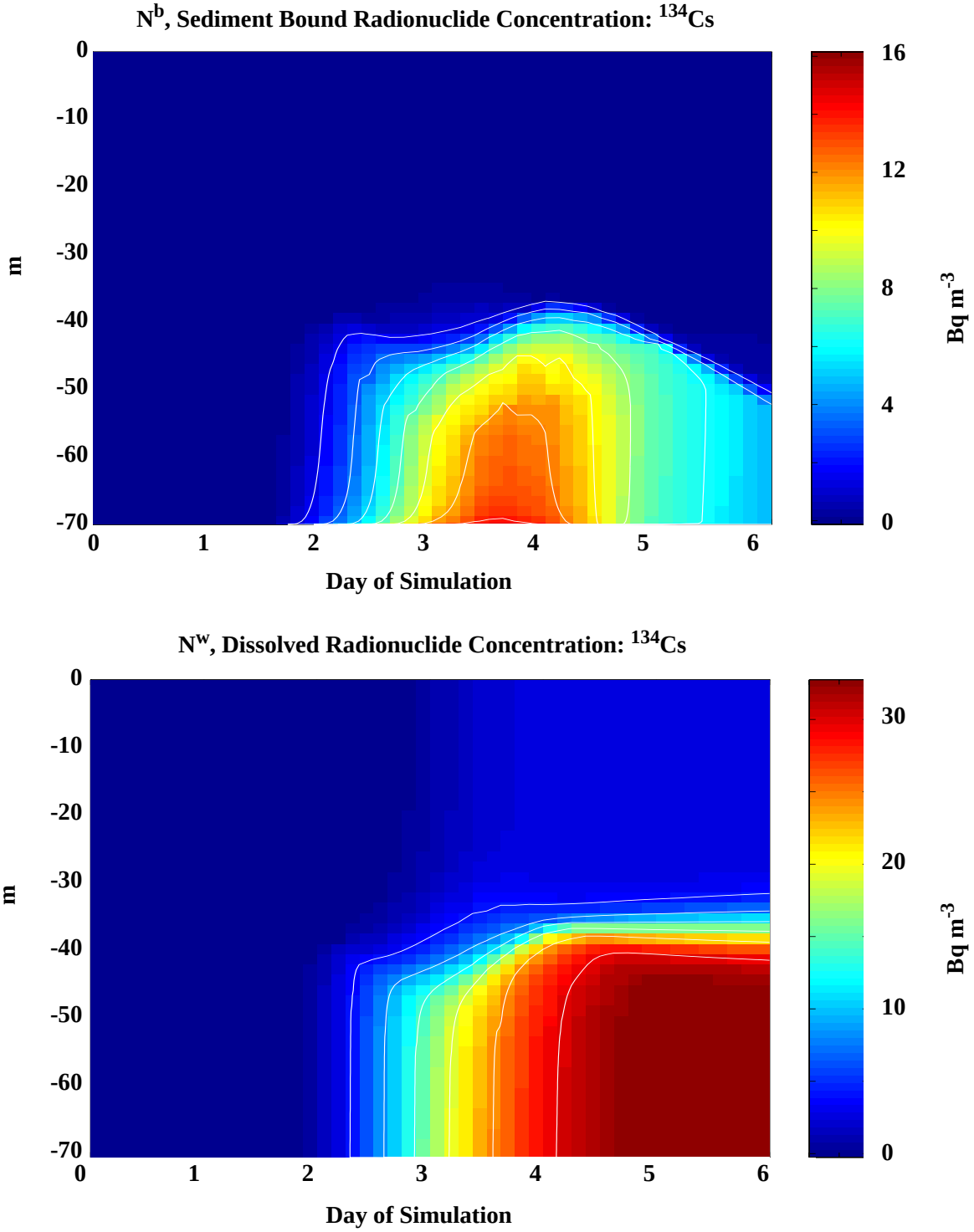

Figure 10. Time - depth contours of bound and dissolved radionuclide concentrations for Run 1, for a radionuclide species (^{134}Cs) with relatively strong binding to sediment ($\bar{K}_d$ = 1000 ml gm^{-1}). The water is initially uncontaminated, overlying sediment with radioactivity of 100 Bq kg^{-1}.

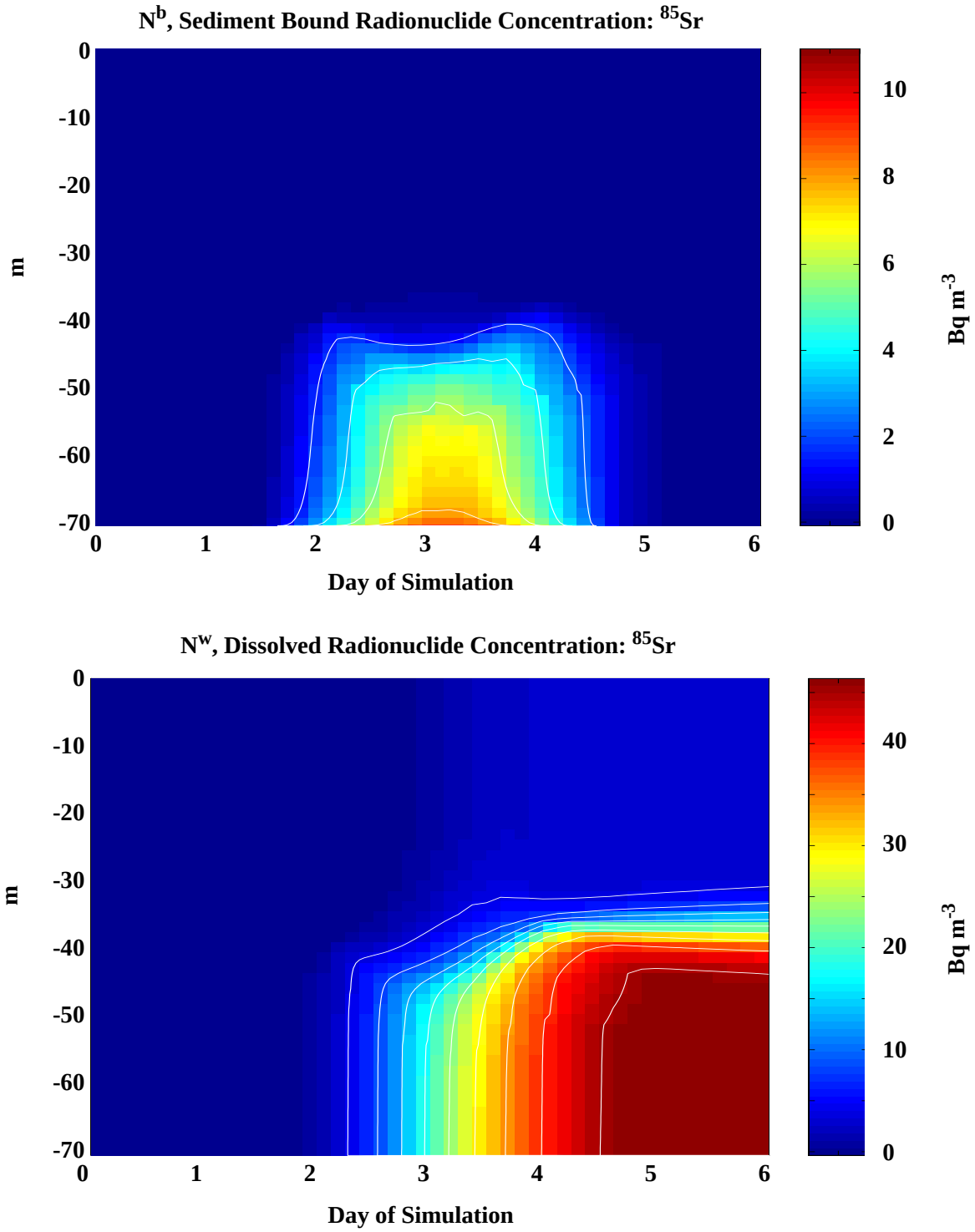

Figure 11. Same as Fig. 10, except, for a radionuclide species (^{85}Sr) with relatively weak binding to sediment ($\bar{K}_d$ = 11 ml gm^{-1}).

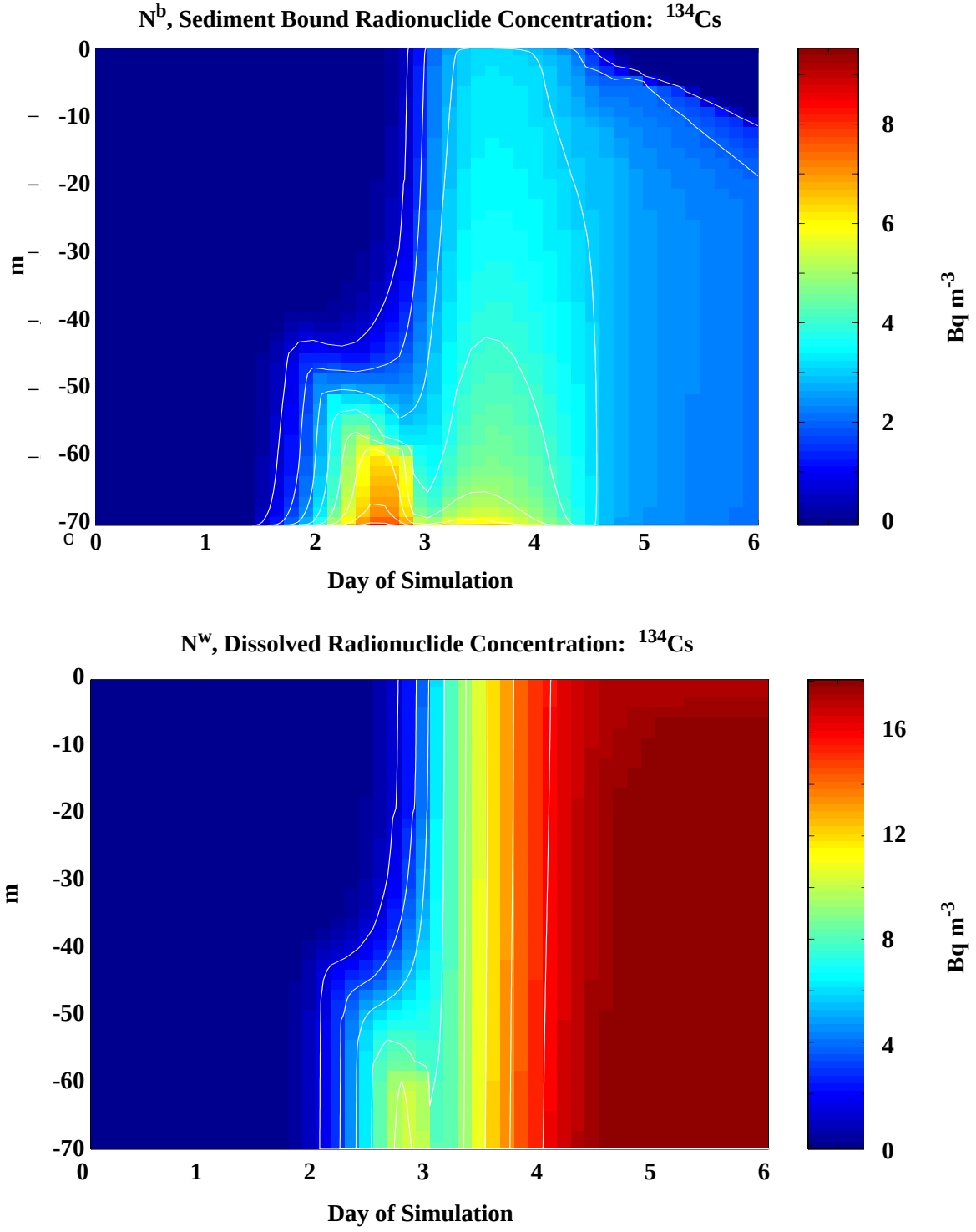

Figure 12. Time - depth contours of bound and dissolved radionuclide concentrations for Run 2, for a radionuclide species (^{134}Cs) with relatively strong binding to sediment ($\bar{K}_d$ = 1000 ml gm^{-1}). The water is initially uncontaminated, overlying sediment with radioactivity of 100 Bq kg^{-1}.

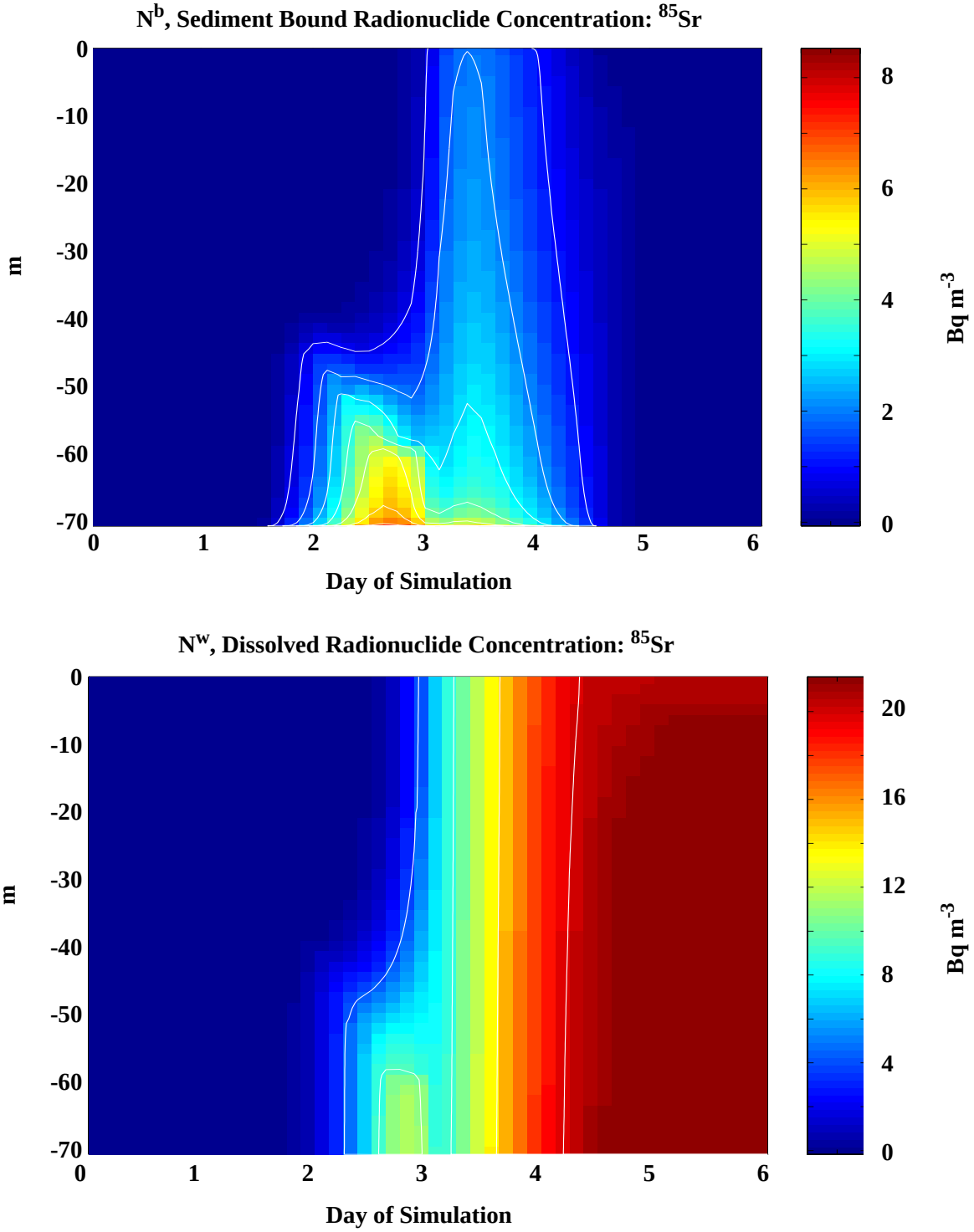

Figure 13. Same as Fig. 12, except, for a radionuclide species (^{85}Sr) with relatively weak binding to sediment ($\overline{K}_d$ = 11 ml gm^{-1}).

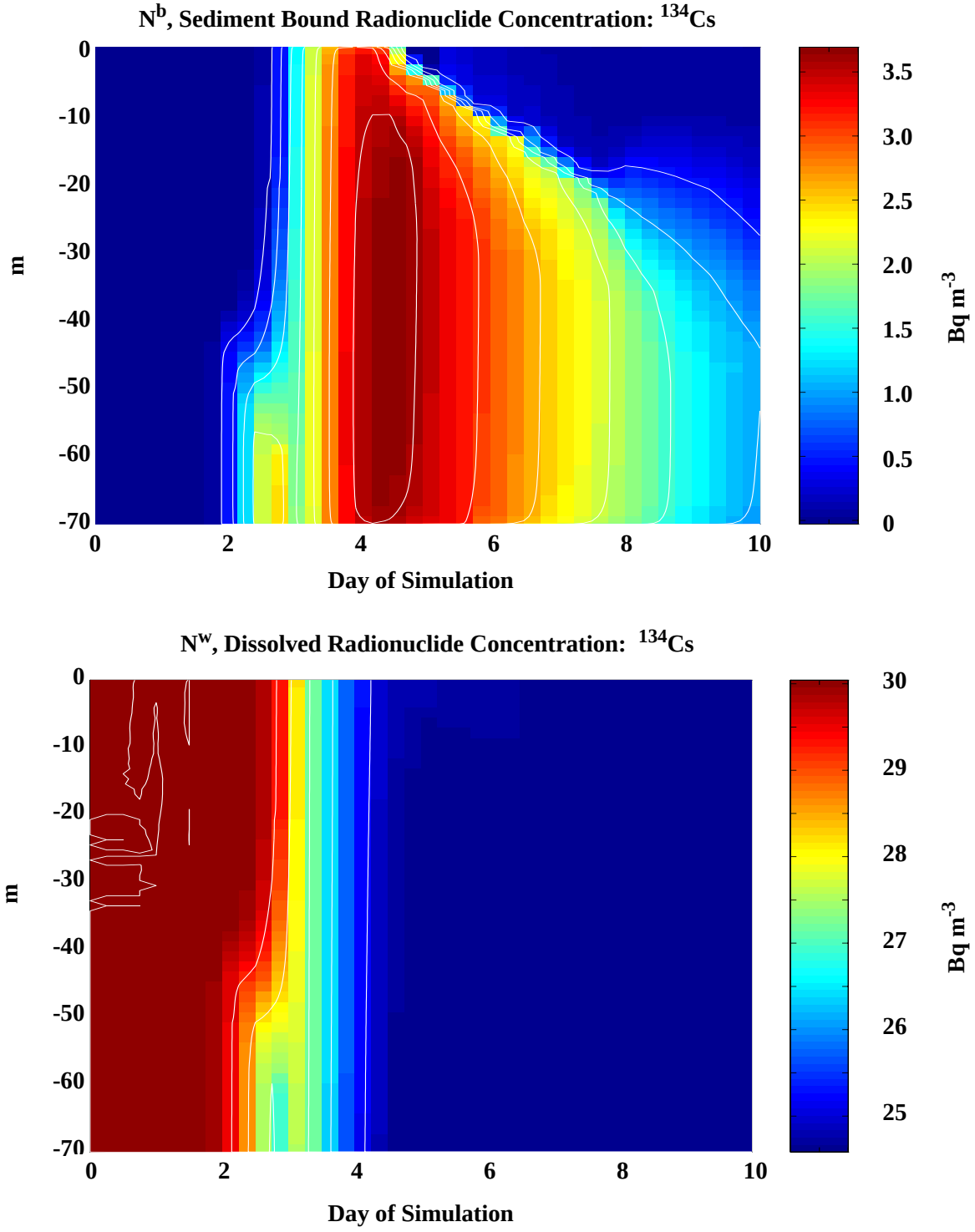

Figure 14. Ten-day simulation with same storm as before except with weak surface and bottom stress after the storm (day 5.5), and initially contaminated water overlying uncontaminated sediment. The radionuclide tracer has relatively strong sediment binding.

References

Ekman, V.W. 1905. On the influence of the earth's rotation on ocean currents, *Ark. Mat. Astr. Fys., 2*, 1-52.

McPhee, M.G., 1979. The effect of the oceanic boundary layer on the mean drift of sea ice: Application of a simple model, *J. Phys. Oceanogr., 9*, 388-400.

McPhee, M. G., 1981. An analytic similarity theory for the planetary boundary layer stabilized by surface buoyancy, *Boundary-Layer Meterol., 21*, 325-339.

McPhee, M.G. 1990. Small scale processes, in: *Polar Oceanography,* ed. W. Smith, 287-334, Academic Press, San Diego, CA.

McPhee, M.G., 1994: On the Turbulent Mixing Length in the Oceanic Boundary Layer, *J. Phys. Oceanogr., 24*, 2014-2031.

McPhee, M. G., 1996. An inertial-dissipation method for estimating turbulent flux in buoyancy driven, convective boundary layers, in press: *J. Geophys. Res*.

Mehta, A. J., 1988. Laboratory studies on cohesive sediment deposition and erosion, in *Physical Processes in Estuaries*, eds. J. Dronkers and W. van Leussen, Springer-Verlag, New York, 427-445.

Oughton, D. H., P. Børretzen, B. Mathinsen, E. Tronstad, and B. Salbu, 1995. Mobilization of radionuclides from sediments: Potential sources to Arctic waters. Unpublished manuscript, Arctic Nuclear Wastes Assessment Project.

Smith, J. D., 1977. Modeling of sediment transport on continental shelves, in E.D. Goldberg, I. N. McCave, J. J. O'Brien and J. M. Steele (eds.), *The Sea, 6*, Wiley, New York, 539-577.

Smith, J. D., and T. S. Hopkins, 1972. Sediment transport on a continental shelf off of Washington and Oregon in light recent current measurements, in *Shelf Sediment Transport*, eds. Swift, Duane, and Pilkey, Dowden, Hutchinson and Ross, Inc., Stroudsberg, PA, 143-180.

Trowbridge, J. H., and G. C. Kineke, 1994. Structure and dynamics of fluid muds on the Amazon continental shelf, *J. Geophys. Res., 99*, 865-874.